MinPlot: A mineral formula recalculation and plotting program for electron probe microanalysis

Jesse B. Walters

Institut für Geowissenschaften, Goethe Universität, Frankfurt am Main, 61348

Disclaimer: This preprint has not been peer reviewed, and a manuscript has been submitted to the journal Mineralogia (http://www.mineralogia.pl/index.html)

MinPlot is available at: https://geojesse.weebly.com/useful-things.html

Abstract

MinPlot is a MATLAB®-based mineral formula recalculation and compositional plotting program for electron microprobe analyses (EPMA). The program offers recalculation and structural formula assignment for 15 different mineral groups: Garnet, pyroxene, olivine, amphibole, feldspar, mica, staurolite, cordierite, chlorite, chloritoid, talc, epidote, titanite, spinel, and sulfides. MinPlot is a fast and easy to use command line program and requires no prior computer programming knowledge. Percent mass fractions of oxides are loaded from datafiles and the user answers simple prompts to select mineral type, normalization scheme, and plotting options. Recalculated mineral formulas are automatically saved as output files and plots may be further manually customized by the user prior to saving. MinPlot can perform thousands of calculations in seconds and the modular nature of the program makes it simple to add new calculation routines in future releases. Finally, MinPlot utilizes simple matrix algebra and linear programing steps, and is thus anticipated to be forwards compatible with future releases of MATLAB®. Combined, these features make MinPlot a powerful and useful program for the processing of EPMA data.

1. Introduction

Electron probe microanalysis (EPMA) is one of the most powerful and commonly used tools for the quantitative determination of mineral compositions. Following analysis, standardization, and corrections for atomic number, absorption, and fluorescence effects, data are reported by the EPMA software as the percent mass fraction (g/g × 100) of oxides (e.g., SiO_2, TiO_2, Al_2O_3, etc) or elements (e.g., Si, Ti, Al, etc). Conversion to the atomic proportions of the mineral formula is necessary for mineral classification and assessment of compositional trends, such as changes of endmember fractions in zoned minerals. Over the years many programs have been offered which convert percent mass fraction of oxides to mineral structural formulae for specific minerals, such as garnet (Grew et al., 2013; Knowles, 1987; Locock, 2008; Yavuz and Yildirim, 2020), pyroxene (Sturm, 2002; Yavuz, 2013), mica (Yavus 2003a, b), chlorite (Yavuz et al., 2015), amphibole (Locock, 2013; Esawi, 2004; Mogessie et al., 1990; Mogessie, 2001; Rao and Rao, 1996; Richard and Clark, 1990; Rock, 1987; Rock and Leake, 1984; Spear and Kimball, 1984; Tindle and Webb, 1994; Yavuz, 2007), and others. Other programs allow for the recalculation of formulae for a variety of mineral species: MINFILE (Afifi and Essene, 1988), MINTAB (Rock and Caroll, 1990), HYPER-FORM (De Bjerg et al., 1992), PASFORM (De Bjerg et al., 1995), CALCMIN (Brandelik, 2009), MINCALC (Bernhard, 2010), and MINERAL (De Angelis and Neill, 2012). While there are many available programs offered over the years, all

established programs have restrictions limiting or entirely preventing their use on modern computing operating systems. Many of these, such as MINCALC, CALCMIN, WinAmphcal, and others, utilize the Visual Basic programming language coupled with Microsoft Excel™; however, the Visual Basic language was abandoned by Microsoft© and these programs may no longer function. Additionally, Visual Basic-based programs can only be operated on Windows™ systems, requiring users of other operating systems to run virtual machines. MINERAL (De Angelis and Neill, 2012) is a powerful MATLAB®-based program which calculates mineral formulae with error propagation, and can recalculate the formulae of feldspar, olivine, pyroxene, spinel, ilmenite, amphibole, garnet, epidote, and mica. While Fe^{3+}-Fe^{2+} estimation is calculated in MINERAL, normalization to 15 or 13 cations for amphibole is only appropriate for some compositions (Leake et al., 1997; Hawthorne et al., 2012). Finally, no program offers options for automated publication-ready plotting of mineral compositions.

Here a new MATLAB®-based command line program, called MinPlot, is presented. MinPlot can perform mineral formula recalculation and automated compositional plotting for garnet, pyroxene, olivine, amphibole, feldspar, mica, staurolite, cordierite, chlorite, chloritoid, talc, epidote, titanite, spinel, and sulfides. Users need no programming experience and MinPlot is functional on any computer capable of running MATLAB®. Importantly, the program offers a flexible approach, with multiple yes-no prompts, allowing the user to choose multiple normalization and plotting schemes where appropriate. Unlike spreadsheet-based approaches, MinPlot can calculate recalculate hundreds to thousands of analyses within seconds. The program is capable of outputting publication-ready compositional diagrams that are commonly used in the literature. The modular approach to the program, which runs on from a central script that calls functions for each mineral, means that the addition of new minerals or normalization procedures in the future requires little modification of the existing programming framework. Finally, the MATLAB® language is forwards compatible and the program will continue to function in the future as the language is updated.

2. Program Design

2.1 General Formula Recalculation Procedure

MinPlot is based around a central script (MinPlot.m), which calls functions for each mineral (*e.g.*, garnet_fe3.m, garnet_fe2.m, etc). Mineral functions differ in their design and complexity, with only a single function for minerals like feldspar and epidote, and up to twelve functions for amphibole. The same basic formula is applied, in linear programming steps, to calculate molar proportions of cations and oxygens, respectively, from the mass fraction of the oxides:

$$n_i^C = \frac{W_j}{m_j} * M_j^C \quad (1)$$

and

$$n_i^{O_2} = n_i^C * \frac{M_j^{O_2}}{M_j^C} \quad (2)$$

Where n_i^C and $n_i^{O_2}$ are the unnormalized moles of cations and O_2, respectively, of element *i* in the analyzed phase, W_j is the measured mass fraction of the oxide *j* (in weight percent), m_j is the molecular weight of the oxide *j*, and M_j^C and $M_j^{O_2}$ are the moles of cations and O_2, respectively, in

the oxide *j*. Molecular weights of the oxides are calculated using the atomic weights using the values reported in the *Atomic weights of the elements 2013 (IUPAC Technical Report)* of Meija *et al*. (2013).

Calculation of the atoms per formula unit (APFU) of each element and their assignment in the structural formula of the mineral follow a normalization procedure based on assumptions of charge balance. While the normalization procedure is specific to each phase, it may generally be summed up as shown in the following. Normalization on an oxygen equivalents basis for some minerals (assuming a fixed number of negative charges) is calculated following Equation 2:

(3) $$NF^{O_2} = \frac{n_{ideal}^{O_2}}{\sum_i^Z n_i^{O_2}}$$

Where NF^{O_2} is the oxygen-based normalization factor, Z is the number of elements, and $n_{ideal}^{O_2}$ is the ideal moles of oxygen (negative charges) per formula unit (*e.g.*, 12 for garnet, 4 for olivine, 6 for pyroxene, etc). For Cl and F-bearing minerals, these elements do not change the formal negative charge are not included in the oxygen sum.

Normalization of garnet, olivine, pyroxene, spinel, and chloritoid uses the method of Schumacher (1991) for Fe^{3+}-Fe^{2+} calculation. Prior to Fe^{3+} estimation, the moles of cations are normalized on a cation basis (assuming a fixed number of positive charges):

(4) $$NF^{C} = \frac{n_{ideal}^{C}}{\sum_i^Z n_i^{C}}$$

Where NF^C is the cation-based normalization factor and n_{ideal}^{C} is the ideal moles of cations (positive charges) per formula unit (e.g., 8 for garnet, 3 for olivine, 4 for pyroxene, etc). For some minerals, such as amphibole, Z is less than the total number of elements and n_{ideal}^{C} is less than an ideal the sum of all the cations. In these cases, the normalization procedure assumes that only certain sites are full and is useful for minerals with structural vacancies. Once the correct normalization procedure is made, the unnormalized moles of cations are multiplied by the normalization factor:

(5a) $n_i^{Norm} = n_i^C * NF^C$

or

(5b) $n_i^{Norm} = n_i^C * NF^{O_2}$

Where n_i^{Norm} is the normalized moles of each cation (in APFU).

Ferric iron calculation follows Schumacher (1991) for garnet, olivine, pyroxene, spinel, and chloritoid. In these cases, the oxygen sum ($\sum_i^Z n_i^{O_2}$) is calculated using the moles of oxygen calculated by Equation 2 following normalization using Equation 5 on a cation basis. The oxygen, or rather charge, deficiency determines the amount of Fe calculated as Fe^{3+}:

(6) $$OD = n_{ideal}^{O_2} - (\sum_i^Z n_i^{O_2})_{cation\ normalized}$$

Where *OD* (oxygen deficiency) must be greater than 1 to calculate Fe^{3+} using charge balance constraints. The amount of Fe^{3+} and Fe^{2+} are calculated as:

(7a) $n_{Fe^{3+}}^{norm} = 2 * OD$

And

(7b) $n_{Fe^{2+}}^{norm} = n_{Fe}^{Norm} - n_{Fe^{3+}}^{norm}$

Where $n_{Fe^{3+}}^{norm}$ and $n_{Fe^{2+}}^{norm}$ are the moles of Fe^{3+} and Fe^{2+} in atoms per formula unit, respectively. If $n_{Fe}^{Norm} > 2 * OD$, then $n_{Fe^{3+}}^{norm}$ is assumed to equal n_{Fe}^{Norm} ($Fe^{3+}/\Sigma Fe$ = 1.0), whereas MinPlot automatically calculates $n_{Fe^{3+}}^{norm} = 0$ if $2 * OD \leq 0$.The oxygen deficiency is output with the structural formula and analyses with negative OD values should not be considered if Fe^{3+} estimation is important. Formula recalculation assuming $\Sigma Fe=Fe^{2+}$ are also available for garnet, pyroxene, and olivine.

2.2 *General approach to structural formula assignment*

Site assignment to the structural formula follows the standard procedure of filling the structurally smallest sites first, such as the tetrahedral site in silicate phases. The tetrahedral sites are not allowed to contain excess Si. For example, if the calculated Si content (APFU) in garnet is less than 3, then the calculated value is used; however, if Si is in excess, then a value of 3 is assigned. Al^{IV} is then assigned: If the tetrahedral site is full, all Al is treated as Al^{VI}, whereas some Al^{IV} may be otherwise assigned. For low Al garnets, such as andradite, all Al could theoretically be Al^{IV}. If 3-Si is greater than the calculated Al content (APFU), then all Al is assumed to be Al^{IV}, otherwise Al^{IV}=3-Si. Ferric iron may also be assigned to the tetrahedral site if the site is not already filled by Al+Si. Assignment of Al to structurally larger sites, such as the octahedral site in garnet, is calculated as Al_{total}-Al^{IV}. A similar calculation is done if ferric iron is partially assigned to the tetrahedral site. This procedure, with or without ferric iron, is followed for tetrahedral site assignment in all silicate phases. Assignment to structurally larger sites in most silicate phases follows a more straightforward procedure, *e.g.* all Mg in garnet is assigned to the dodecahedral site, and maximum site assignments are not imposed. The sum of the site occupancies should be checked by the user to ensure the quality of the analysis. The order and method of site assignment for specific phases is given in the scripts for each phase, with worked examples for each phase given in Table S1.

2.2 Loading and Saving Data

MinPlot reads data stored as text (.txt) files. The first line must contain oxide-based headers that are specific to the mineral formula to be recalculated (see Table 1). The headers must have capital and lowercase characters as shown in Table 1. For some phases, certain oxides are optional and will be calculated assuming a mass fraction of zero ($W_j = 0$) if they are not included in the file read by MinPlot. MinPlot searches the header row for the column containing the appropriate header for each oxide, as a result the oxide data can be listed in any order in the input file. To start MinPlot, change the MATLAB® directory to the folder containing MinPlot and type the name of the program into the command window and hit 'return'. When loading the data, the user is prompted to select the file in a pop-up window and, importantly, the file can be located in any folder on the user's computer or in their network. Following calculation, the user is prompted to save their calculation. If yes, the data is automatically saved as tab delimited text files in the same directory as the source file, allowing for simplified data organization.

2.3 Plotting Data

Automated plotting of compositional data is available for most minerals and the user may select which types of plots they want to make for the mineral of interest. A select set of options are available for symbol type (circle, square, diamond, triangle), color (blue, orange, yellow, purple, green, cyan, and red), and symbol size (a non-dimensional scalar value, input values

Table 1. The following oxides (in wt. %) are either required (green) or optional (yellow) in the data file read by MinPlot.

Mineral	Oxides SiO_2	TiO_2	Al_2O_3	Cr_2O_3	Y_2O_3	NiO	ZnO	Fe_2O_3	FeO	MnO	MgO	CaO	Na_2O	K_2O	BaO	F	Cl
Garnet																	
Pyroxene																	
Olivine																	
Feldspar																	
Epidote*																	
Clinoamphibole																	
Mica																	
Staurolite																	
Chlorite																	
Chloritoid																	
Cordierite																	
Talc																	
Titanite																	
Spinel																	

*Need to include either FeO or Fe2O3, not both.

between 50-200 are appropriate for most practical applications). Plots are not automatically saved. Instead, the variety of potential file types (*e.g.*, .pdf, .png, .jpg, etc), degree of compression, manual modification the figure prior to saving (*e.g.*, adjustment of colors, widths, etc), and choice of a vector- or raster-based image format, offered by MATLAB® give the user more flexibility when saving plots manually. For example, saving plots as a vector-based PDF allows the user to modify the plots in a vector graphics editor program prior to publication.

3. Calculation and Plotting Routines

Below the mineral-specific recalculation procedures and plotting are described. Note that all plots are resized by 50 to 60 % and the font is changed to match journal specifications; however, the plots are otherwise unchanged from the MinPlot output. Tables of worked examples of literature data recalculated in MinPlot are given in supplementary Table S1.

3.1 Garnet

Garnet ($X_3Y_2Z_3O_{12}$) has a flexible structure and can incorporate a variety of elements in its four atomic sites (Grew et al., 2013). Here the compositional space is restricted to those elements which are abundant in most natural garnets and can be measured on the EPMA: Na, Ca, Ca, Mg, Mn, Fe^{2+}, and Y on the dodecahedral (X) site, Fe^{3+}, Cr, Ti, and Al on the octahedral (Y) site, Fe^{3+}, Al, and Si on the tetrahedral (Z) site, and O_2 on the anion site. Garnet structural formula are calculated using normalization to 8 cations and 12 oxygens (for Fe^{3+}-estimation), or 12 oxygens alone (for $\Sigma Fe=Fe^{2+}$). Endmember fractions are calculated using the matrix inversion method for solving systems of linear equations:

(8) $X_{Endmembers} = M^{-1} \cdot A_T$

Where $X_{Endmembers}$ is the matrix of endmember fractions, M^{-1} is a matrix of the ideal moles of the cations for each endmember, and A_T is the transposed matrix of Ca, Mg, ΣFe, Cr, Mn, and Al for each analysis. Following Equation 8, the sum of the endmembers is calculated and normalized to unity. Equation 8 is convenient for rapidly solving large systems of linear equations; however, only square matrices are invertible, and the technique is not appropriate for all endmember

calculations. The garnet endmembers considered are almandine (X_{Alm}), spessartine (X_{Sps}), grossular (X_{Grs}), pyrope (X_{Prp}), andradite (X_{And}), and uvarovite (X_{Uv}).

Plotting options for garnet include the X_{Alm} + X_{Sps}, X_{Grs}, and X_{Prp} ternary (Fig. 1A). It is important to note that X_{Sps} and X_{Alm} do not perfectly co-vary, especially at low P-T conditions near the garnet-in reaction (e.g., Caddick and Kohn, 2013), and restricting the 4-dimensional endmember composition space of common garnets to 3-dimensions will obscure compositional trends. A second Fe^{3+}, Cr, and Al^{VI} ternary diagram for substitutions on the octahedral site is also available (Fig. 1B).

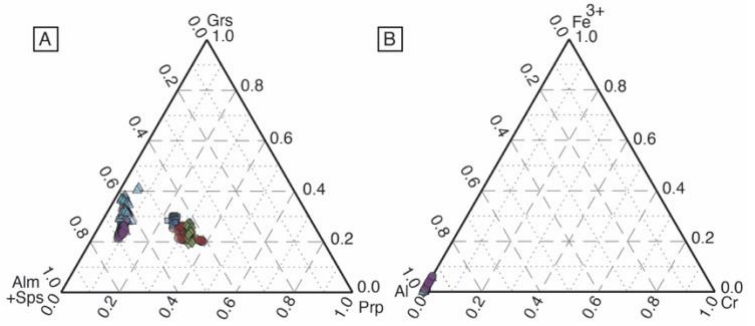

Figure 1. Ternary X_{Alm} + X_{Sps}, X_{Grs}, and X_{Prp} (**A**), and Fe^{3+}, Al, and Cr (**B**) garnet compositional diagrams. Example garnet data are from Walters et al. (2019; 2021): Light blue triangles – garnet blueschist (DR1203-11-03; Dominican Republic), purple circles – garnet-omphacite-chlorite fels (SY462; Syros, Greece), red circles – metagabbroic eclogite (G083-12; Vendée, France), dark blue squares – eclogite (SVS-11-01; Svetlik-Sus, Czech Republic), and green diamonds – eclogite (TIS-11-02; Tisova, Czech Republic).

3.2 Pyroxene

Pyroxene ($M2M1T_2O_6$) compositions are calculated following Morimoto et al. (1989), with K, Na, Ca, Fe^{2+}, and Mg on the distorted octahedral M2 site, Fe^{2+}, Mg, Mn, Cr, Fe^{3+}, Ti, and Al on the octahedral M1 site, and Fe^{3+}, Al, and Si on the tetrahedral site. Vanadium, Zn, and Sc may also substitute into the M1 site, typically observed at trace levels, and Li may substitute into M2 as a major element in spodumene but is not measurable by EPMA. These elements are not considered here. Endmember fractions are calculated using Equation 7 for wollastonite (X_{Wo}), ferrosillite (X_{Fs}), enstatite (X_{En}), jadeite (X_{Jd}), aegirine (X_{Aeg}), and kosmochlore (X_{Kos}). Normalization is to 4 cations and 6 oxygens in the Fe^{3+}-estimation routine, and on a 6-oxygen basis for $\Sigma Fe=Fe^{2+}$.

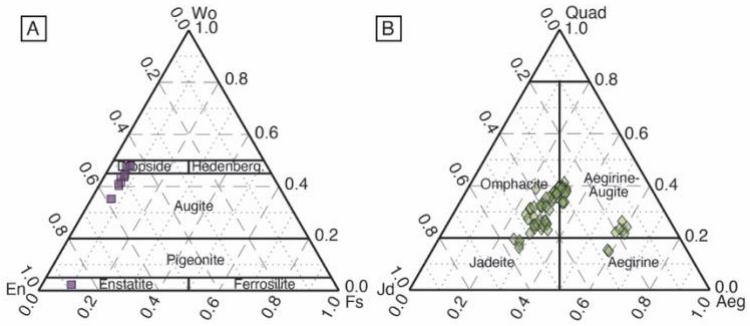

Figure 2. Ternary X_{Wo}, X_{Fs}, and X_{En} (**A**), and X_{Quad}, X_{Jd}, and X_{Aeg} (**B**) pyroxene compositional diagrams. Example data in **A** are clino- and orthopyroxene grains from gabbro-norite cumulate bodies and dikes from Alpine-Apennine ophiolites (Piccardo and Guarnieri, 2011), whereas example data in **B** are Na-clinopyroxene from a metasomatic garnet-omphacite-chlorite fels from Syros, Greece (SY462; Walters et al., 2019; 2021).

Plotting and classification also follows Morimoto et al. (1989). First, the so called 'Q-J' diagram distinguishes Ca-Mg-Fe pyroxenes (Quad), Na-Ca pyroxenes (Na-Ca), and Na pyroxenes (Na), where J=2Na is plotted on the x-axis and $Q=Ca+Mg+Fe^{2+}$ is plotted on the y-axis (see Fig. S1). For Ca-rich pyroxenes, the user may restrict endmember calculation and plotting to 'Quad' compositions, which is a useful approximation for many igneous pyroxenes. Discrimination plots also include the X_{Wo}, X_{Fs}, and X_{En}, (Fig. 2A) and X_{Quad}, X_{Jd}, and X_{Aeg} (Fig. 2B) ternaries after Morimoto et al. (1989).

3.3 Olivine

Olivine (M_2TO_4) is calculated here with Ca, Mg, Mn, Fe^{2+}, Ni, Cr, Fe^{3+}, Ti, and Al on the octahedral M site, and Fe^{3+}, Al, and Si on the tetrahedral site. Normalization is to 3 cations and 4 oxygens in the Fe^{3+}-estimation routine, and on a 4 oxygen basis for $\Sigma Fe=Fe^{2+}$. Endmember fractions are calculated for forsterite (X_{Fo}), fayalite (X_{Fa}), tephroite (X_{Te}), and larnite (X_{Lrn}). Three plots are available for olivine (Fig. 2). First is an option for a binary plot of the forsterite content (Fig. 3A), where the user is prompted to specify the upper and lower Fo limits. Second, a ternary diagram in the X_{Fo}, X_{Lrn}, and X_{Fa} + X_{Te} system is available (Fig. 3B). Finally, a plot with the Fo number on the x-axis and mass fraction of NiO (wt. %) on the y-axis is available (Fig. 3C).

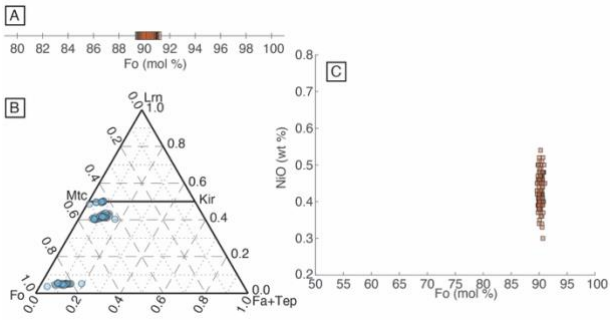

Figure 3. Binary Fo number (**A**), ternary X_{Fo}, X_{Lrn}, and X_{Fa} + X_{Te} (**B**), and Fo number vs. NiO (wt %) (**C**) olivine compositional diagrams. Data in **A** and **C** are analyses of olivine from mantle peridotite, Wadi Fins, Oman (de Obseso and Kelemen, 2020), whereas data in **B** are analyses of experimentally grown olivine (Le Pioufle and Canil, 2012).

3.4 Amphibole

Amphibole ($AB_2C_5T_8O_{22}W_2$) has a complex structure with a wide compositional space. MinPlot follows the recommendations of Leake et al. (1997) and Hawthorne et al. (2012) for structural assignment, with □, K, Na, and Ca on the A site, Ca, Na, Mn, Fe^{2+}, and Mg on the B site, Mn, Fe^{2+}, Mg, Fe^{3+}, Cr, Ti, and Al on the C site, Si and Ti on the T site, and OH^-, F^-, Cl^-, and O^{2-} on the W site. Minor elements, such as Pb, Zn, Co, V, Sc, and Zr, often have contents at or below the EPMA detection limit and are not included. Additionally, Li and Be cannot be measured by EPMA and are also excluded. For a more complete formula recalculation and classification of amphiboles, including Li and other minor elements, see Locock (2014).

Amphibole formula recalculation presents multiple challenges, particularly estimation of Fe^{3+}-Fe^{2+} and the occupancy of the W-site. The calculation procedure here follows the IMA recommendations of Hawthorne et al. (2012) and Locock (2014). The procedure is summarized here. Amphibole is commonly normalized on the basis of 24(O,OH,F,Cl) where occupancy of the W-site is $(OH,F,Cl)_W$ = 2 APFU when H_2O is not analyzed. However, substitution of Ti in the M1 site is often balanced by incorporation of O^{2-} (Oberti et al., 1992):

(9) $Ti_{M1}^{4+} + 2O_W^{2-} \rightarrow (Mg, Fe^{2+})_{M1} + 2(OH)_W^-$

As a result, $(OH,F,Cl)_W$ can be calculated as (2 - 2Ti) APFU, thus correcting for the maximum possible contribution of O^{2-} on the W-site (Hawthorne et al., 2012). This assumes that Ti_{M3} and Ti_{M2} are negligible, which is not always the case (see Tiepolo et al., 1999). MinPlot allows the user to choose formula recalculation assuming $(OH,F,Cl)_W$ = 2 APFU or with the Ti-O^{2-} correction.

Ferric iron estimation can be calculated through normalization to sets of cation sums which provide lower and upper $Fe^{3+}/\Sigma Fe$ limits (Leake et al., 1997; Hawthorne et al., 2012). It is important to note that stoichiometric estimation of Fe^{3+}-Fe^{2+} requires all major cations to be analyzed and is thus not appropriate here for Li-rich compositions. Additionally, Fe^{3+}, like Ti, may be charge balanced by dehydrogenation on the W site, which is not considered in MinPlot. The

Fe^{3+}-Fe^{2+} calculation procedure is as follows. First, the all-ferrous formula is calculated to give the maximum number of cations. Lower $Fe^{3+}/\Sigma Fe$ limits are calculated from the all-ferrous formula based on the three following criteria:

(1-1) Si ≤8 APFU

(1-2) $(Si + Al + Ti + Fe^{2+} + Fe^{3+} + Mn + Mg + Ca + Na + K) \leq 16$ APFU

(1-3) $(Si + Al + Ti + Fe^{2+} + Fe^{3+} + Mn + Mg + Ca) \leq 15$ APFU

Criteria 1-1 and 1-2 are set by the structure. There cannot be more than 8 Si cations on the T site or 16 total cations. Criterion 1-3 assumes that Ca does not incorporate into the A-site, which may not be true in amphiboles from Ca-rich rocks, like marbles and calc-silicates (Hawthorne et al., 2012). If none of these criteria are invalidated, the minimum Fe^{3+} estimate comes from the all-ferrous formula. The upper $Fe^{3+}/\Sigma Fe$ limits are calculated using the five following criteria:

(2-1) $(Si + Al) = 8$ APFU

(2-2) $(Si + Al + Ti + Fe^{2+} + Fe^{3+} + Mn + Mg + Ca + Na) = 15$ APFU

(2-3) $(Si + Al + Ti + Fe^{2+} + Fe^{3+} + Mn + Mg) = 13$ APFU

(2-4) (Si + Al + Ti + Cr + Fe^{3+}) = 10 APFU

(2-5) $\Sigma Fe=Fe^{3+}$

Criterion 2-1 assumes that Si and Al only substitute on the T site, whereas criterion 2-2 assumes that only K substitutes on the A site. Hawthorne et al. (2012) warn that criteria 2-1 and 2-2 are not appropriate for richterite compositions where Ti may occur as a T cation and K may substitute on the B site. Criterion 2-3 assumes that Fe^{2+}, Mn, or Mg substitute on the on the C site, which may be violated if these elements also substitute on the B site. Criterion 2-4 assumes that 3+ and 4+ cations fill the T and M2 sites, and the normalization factor is calculated as 36/(46-Si-Ti-Al-Cr) (Leake et al., 1997). Criterion 2-4 is important for Na-rich amphibole and is not included in the spreadsheet of Locock (2014). Finally, an all-ferric formula provides the extreme upper $Fe^{3+}/\Sigma Fe$ limit.

MinPlot automatically selects the appropriate lower and upper Fe^{3+} limits. The lower limit is selected as the criterion which gives the minimum normalization factor; however, if all the normalization factors have values greater one, then the $\Sigma Fe=Fe^{2+}$ formula provides the lower limit. Additionally, if the three minima criteria have normalization factors which are lower than those for the four maximum criteria, then Fe^{3+} cannot be estimated and the $\Sigma Fe=Fe^{2+}$formula is output. In contrast, the maximum normalization factor provides the best estimate for the upper $Fe^{3+}/\Sigma Fe$ limit. After the upper and lower limits are chosen, MinPlot calculates the median composition between these limits (Leake et al., 1997; Hawthorne et al., 2012).

Amphibole analyses are automatically assigned to plots for Ca ($Ca_B/(Ca+Na)_B \geq 0.75$), Na-Ca ($0.75 > Ca_B/(Ca+Na)_B > 0.25$), and Na ($Ca_B/(Ca+Na)_B \leq 0.25$) groups. The classification scheme of Hawthorne et al. (2012) is used: Amphibole compositions are plotted as $(Al + Fe^{3+} + 2Ti)_C$ on the x-axis and $(Na + K + 2Ca)_A$ on the y-axis (Figs. 4A, 4C, and S2). There are two problems with this classification, 1. It is very sensitive to the estimated Fe^{3+} content and 2. The compositional space of the Fe^{2+} endmembers is not explored (e.g., classification of amphibole as actinolite and riebeckite is not possible). For these reasons, MinPlot includes the Si (APFU) vs.

X_{Mg} and Fe^{3+} /(Al + Fe^{3+} + Ti) vs. Fe^{2+}/(Fe^{2+} + Mg + Mn) classification plots for Ca-amphiboles and Na-amphiboles, respectively (Fig. 4 B and D). Additionally, a plot of ΣFe (APFU) vs Fe^{3+}/ΣFe is available, which can be useful for tracking changes in Fe^{3+} content with overall changes in Fe content. Currently plotting options for orthoamphibole are not available.

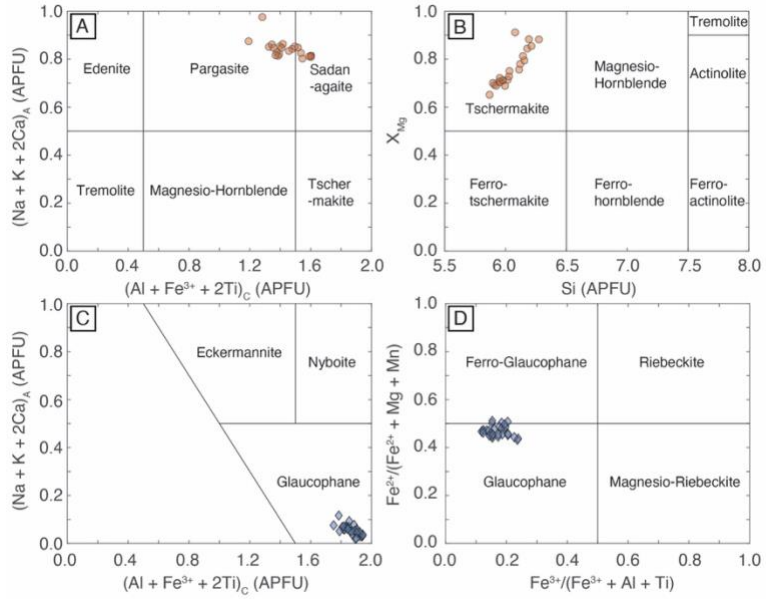

Figure 4. Clinoamphibole compositional and classification diagrams (after Hawthorne *et al*., 2012; Leake *et al*., 1997): (**A**) (Al + Fe^{3+} + 2Ti)$_C$ vs (Na + K + 2Ca)$_A$ diagram for Ca-amphibole, (**B**) Si vs X_{Mg} diagram for Ca-Amphibole, (**C**) (Al + Fe^{3+} + 2Ti)$_C$ vs (Na + K + 2Ca)$_A$ diagram for Na-amphibole, and (**D**) Fe^{3+}/(Fe^{3+} + Al + Ti) vs Fe^{2+}/(Fe^{2+} + Mg + Mn) diagram for Na-amphibole. Analyses of glaucophane are collected on blueschists from Port Macquarie, Australia (PMQ065), whereas Ca-amphibole analyses are collected on zoned amphibole from a retrogressed eclogite from Svetlik-Sus, Czech Republic (SVS-11-01; Walters et al., 2019; 2021).

3.5 Feldspar

Feldspar (AT_4O_8) is calculated here by normalizing to 8 oxygen equivalents, with Ca, Na, K, Ba, Fe^{2+}, Mn, and Mg on the A site and Al and Si on the tetrahedral site (T). Endmembers are calculated for anorthite (X_{An} = Ca/(Ca + Na + K)), albite (X_{Ab} = Ca/(Ca + Na + K)), and alkali feldspar (X_{Or} = K/(Ca + Na + K)). Plotting is available as the classic An-Ab-Or feldspar ternary, with and without subdivisions (Fig. 5). When feldspar subdivisions are selected, the fields for the discredited feldspar intermediate species are plotted: bytownite (Bytw, X_{An} = 70-90), labradorite (Labr, X_{An} = 70-90), andesine (Ands, X_{An} = 30-50), oligoclase (Olig, X_{An} = 10-30), and anorthoclase (Ano, X_{Or}= 10-36). Boundaries for the feldspar subdivision are often drawn either, 1. Maintaining a fixed X_{An} and X_{Or}, or 2. Maintaining constant proportion of X_{An}:X_{Ab} at varying X_{Or} and constant proportion of X_{Or}:X_{Ab} at varying X_{An}. Here the latter is chosen, and the subdivision boundaries are not parallel to X_{An} and X_{Or} (Fig. 5).

3.6 Mica

Mica ($IM_{2\text{-}3}T_4O_{10}W_2$) is calculated here normalizing to 11 oxygen equivalents. Ions are assigned as □, K, Na, Ca, and Ba on the I site, Mg, Mn, Fe^{2+}, Cr, Ti, and Al^{VI} on the M site, Al^{IV} and Si on the tetrahedral T site, and F, Cl, and OH are assigned to the W site. While a major constituent the I site in some micas, Li is not considered here as it is not commonly measured. For micas ΣFe is assumed to be Fe^{2+} for the following reasons: 1. Vacancies are possible at both the octahedral and 12-fold coordinated interlayer sites and 2. The estimation of Fe^{3+} by charge balance requires stoichiometric limits to be exceeded, which is rarely the case for micas (Schumacher, 1991). Li *et al.* (2020) proposed a new method of Fe^{3+} estimation of biotite, using a machine learning-based principal component regression; however, Forshaw and Pattison (2021) found the method to be wildly inaccurate and it is not included in MinPlot. It is also important to note that

the OH content calculated in MinPlot assumes a full W site (OH = 2 – F – Cl), which may not be accurate and thus provides an estimation of the maximum possibly OH content.

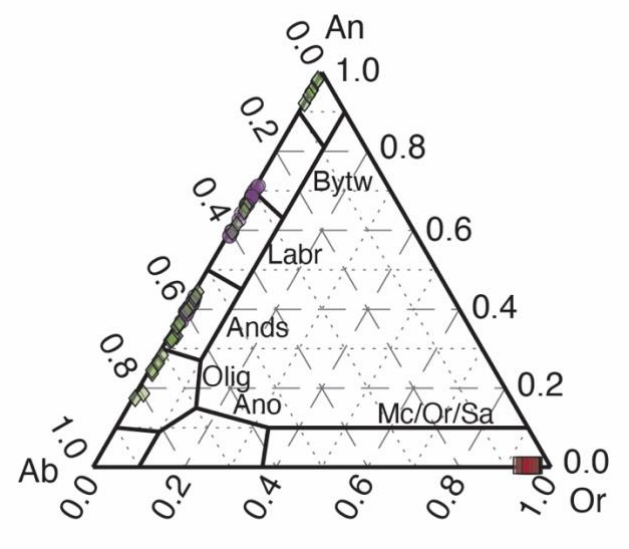

Figure 5. Feldspar anorthite, orthoclase, and albite ternary diagram with compositional subdivisions. Analyses of alkali feldspar (red squares) and plagioclase (purple circles) are from metamorphosed calc silicate rocks from western Maine, USA (SSP18-1A; Walters et al., 2022), as well as plagioclase (green diamonds) from metamorphosed calc silicate rocks from central Nepal (Walters and Kohn, 2017).

Mica endmembers are calculated based on two compositional groups: 1. Dioctahedral muscovite (X_{Ms}), ferroceladonite (X_{FeCel}), magnesioceladonite (X_{MgCel}), paragonite (X_{Pg}), and margarite (X_{Mrg}) species, or 2. Trioctahedral, phlogopite (X_{Phl}), annite (X_{Ann}), eastonite (X_{Eas}), and siderophyllite (X_{Sid}) species. The total dioctahedral or trioctahedral components are given as X_{DiOct} and X_{TriOct}, respectively. The calculation procedure is as follows. First, if the sum of the M site is greater than 2, then some trioctahedral component is possible and is calculated as $X_{TriOct} = \Sigma M - 2$. The dioctahedral endmembers are then calculated using Eqn. 7, as the composition matrix is square (5 linear equations and 5 cations). The matrix of the endmembers proportions is then normalized to the sum of the dioctahedral endmembers plus the trioctahedral component, so that the proportions of the dioctahedral endmembers and the sum of the trioctahedral endmembers sums to unity. The sum of the dioctahedral components is then calculated as $X_{DiOct} = 1 - X_{TriOct}$. The total fraction for the phlogopite-annite join is calculated as $X_{PhlAnn} = Si - 2$ such that individual fractions of phlogopite and annite can be calculated: $X_{Phl} = X_{PhlAnn} \cdot X_{Mg}$ and $X_{Ann} = X_{PhlAnn} - X_{Phl}$. The total fraction for the siderophyllite-eastonite join is also calculated, $X_{SidEast} = 1 - X_{PhlAnn}$, and the individual fractions for eastonite and siderophyllite are calculated: $X_{East} = X_{SidEast} \cdot X_{Mg}$ and $X_{Sid} = X_{SidEast} - X_{East}$. Finally, the fractions are normalized such that the proportions of the trioctahedral endmembers and the sum of the dioctahedral endmembers are equal to 1. Plots for micas include the X_{Pg}, $X_{Ms}+X_{Cel}$, and X_{Mrg} ternary (Fig. 6a), celadonite and muscovite + paragonite solid solution diagram (Fig. 6b), F-Cl-OH ternary (Fig. 6c), and trioctahedral Ann-Phl-Sid-East solid solution diagram (Fig. 6d). The endmember calculation and plotting schemes proposed here assume simple exchange vectors between endmembers and are useful but remain semi-quantitative.

3.7 Staurolite

Staurolite ($A_4B_4C_{18}D_4T_8O_{40}X_8$) exhibits a complex formula with vacancies on multiple sites: Fe^{2+}, Mg, and □ on the A site, Fe^{2+}, Zn, Co, Mg, Li, Al, Fe^{3+},Mn, and □ on the B site, Al, Fe^{3+}, Cr, V, Mg, and Ti on the C site, Al, Mg, and □ on the D site, Si and Al on the T site, and OH, F, and O^{2-} on the X site (Hawthorne *et al.*, 1993). Meaningful estimation of Fe^{3+}, OH, and vacancies in the absence of a full quantitative analysis of all elements is not possible. Instead, the composition space in MinPlot following formula recalculation is restricted to Li, Mg, Mn, Zn, Fe^{2+}, Fe^{3+}, Al, Ti, and Si. The user may select a ratio for $Fe^{3+}/\Sigma Fe$ before normalization. The values of 0.035 for ilmenite-bearing rocks ($X_{Hem} < 0.10$) and 0.070 for hematite-ilmenite rocks ($X_{Hem} >$

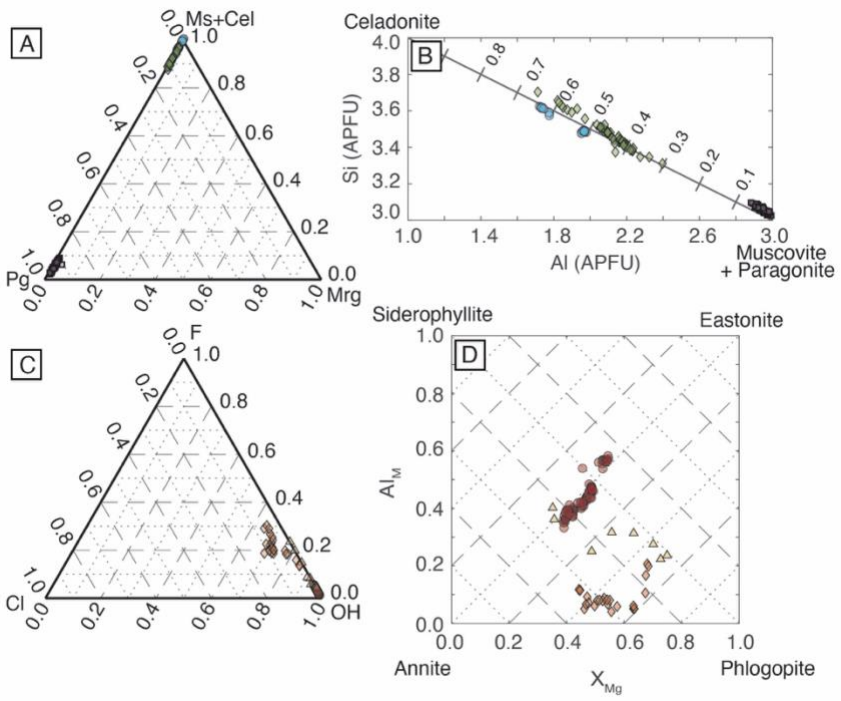

Figure 6. Compositional diagrams for dioctahedral (**A** and **B**) and trioctahedral (**D**) micas: (**A**) muscovite + celadonite, margarite, and paragonite ternary diagram, (**B**) Al vs Si diagram showing binary mixing between muscovite + paragonite and celadonite, (**C**) F, OH, and Cl ternary diagram for substitutions on the hydroxyl (W)-site, and (**D**) X_{Mg} vs Al_M with isolines showing fractional mixing between annite, siderophyllite, eastonite, and phlogopite endmembers. Analyses plotted in **A** and **B** were collected on phengite (light blue circles) in a blueschist from Port Macquarie, Australia (PMQ065; Walters et al., 2019; 2021), and phengite (green diamonds) and paragonite (purple squares) from an ultrahigh pressure metapelite from the Tian Shan, western China (Xu et al., 2022). Biotite analyses, plotted in **C** and **D**, were conducted on grains in a garnet mica schist from western Maine, USA (red circles; Walters et al., 2022), granulite facies para- and orthogneiss (orange diamonds; Spreitzer et al., 2021), and calc silicate rocks from central Nepal (yellow triangles; Walters and Kohn, 2017).

0.10) following Holdaway et al. (1991) are recommended. Normalization is conducted assuming Si + Al – 1/3Li + 2/3Ti + Fe^{3+} = 25.55 APFU following Holdaway et al. (1991). Staurolite often contains non-trivial amounts of Li, with an average of 0.20 APFU (Holdaway et al., 1991). Since Li is not measurable by EPMA, the first normalization step does not consider Li. Successive iterations of normalization, including Li, are conducted until a value of Li = 0.20 APFU is achieved. The total number of vacancies is then calculated as vac = 30-cation total (Holdaway et al., 1991). Further site assignment, endmember calculation, and plotting is not conducted due to the complexity of the structure.

3.8 Cordierite

Cordierite ($A_{0\text{-}1}B_2T2_3T1_6O_{18}$) is calculated here normalized to 18 moles of oxygen equivalents. Cations are assigned as Ca, Na, and K on A, Fe^{2+}, Mn, and Mg on the octahedral B site, Al and Ti on the tetrahedral T2 site, and Si and Al on the tetrahedral T1 site. The fraction of magnesium (X_{Mg}) is calculated as Mg/(Mg+Fe). The incorporation of Fe^{3+} is charge balanced by the substitution of Na within the center of the six-membered rings of the cordierite structure (Deer, Howie, and Zussman, 2013). MinPlot assumes ΣFe = Fe^{2+}, which is not appropriate for rare Na-rich cordierite.

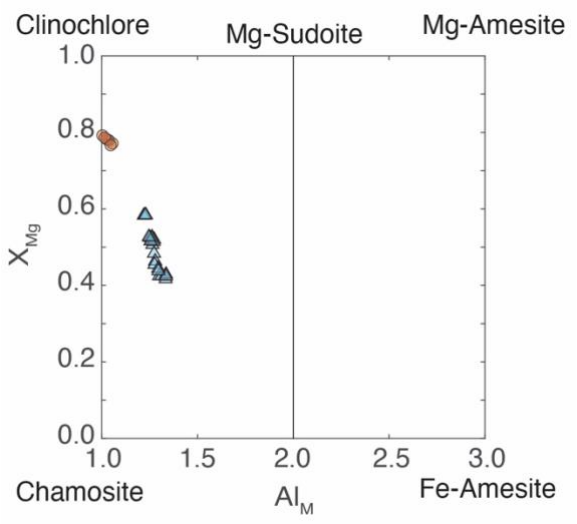

Figure 7. Chlorite compositional diagram with Al_M plotted on the x-axis and X_{Mg} plotted on the y-axis. The compositions of the chamosite, clinochlore, Mg-sudoite, Mg-amesite, and Fe-amesite endmembers are shown. Fe-sudoite would plot Al_M=2.0, X_{Mg}=0.0, but is not listed on the figure. Analysis of chlorite grains from a chlorite schist black wall sample (SY404) collected on Syros, Greece, are shown as orange circles, whereas chlorite analyses from a metasomatic garnet-omphacite-chlorite fels (SY462) from the same locality are shown as blue triangles (Walters et al., 2019; 2021).

3.9 Chlorite

Chlorite ($M_6T_4O_{10}(OH)_8$) is normalized to 14 oxygen equivalents. Cations are assigned as Mg, Mn, Fe^{2+}, Ni, Ti, and Al^{VI} on the octahedral (M) site, whereas Al^{IV} and Si are assigned to the tetrahedral (T) site. In low-Fe chlorite, Fe^{3+} substitution may be dominantly the result of exchange with Al, resulting in a fictive Fe^{3+}-rich Mg-amesite endmember (Masci *et al.*, 2019). Second, the exchange vector $\square^{VI}+2^{VI}R^{3+}=3(Mg,Fe^{2+})^{VI}$ may induce vacancies where R^{3+} is Al or Fe^{3+}. Masci *et al.* (2019) show that a third substitution, following the exchange vector (Fe^{2+}, Mg) + H^+ = Fe^{3+}, may be the primary mechanism behind elevated Fe^{3+} in Fe-rich chlorite. It is possible that other elements, such as Al or Cr, may also substitute via deprotonation. As a result, fully quantitative structural assignment and endmember determination requires the direct analysis of Fe^{3+}, as well as OH and/or O_2. These structural complexities preclude Fe^{3+} estimation by charge balance, and here MinPlot assumes $\Sigma Fe = Fe^{2+}$. Chlorite compositions are plotted in a diagram of Al^{IV} vs X_{Mg}, which explores the compositional space between the clinochlore, chamosite, Mg-sudoite, Fe-sudoite, Mg-amesite, and Fe-amesite endmembers (Fig. 7). Like micas, the chlorite compositional plot assumes simple exchange vectors and does not explore the full compositional space or account for Fe^{3+}, which may be significant in some chlorite. Nevertheless, the plot is useful monitor for compositional variability.

3.10 Chloritoid

Chloritoid is made up of two octahedral layers, L1 and L2, linked by SiO_4 tetrahedra, where L1 is (Na, Ca, Mg, Mn, Fe^{2+})$_2$(Al,Ti,Fe^{3+})$O_2(OH)_4$, L2 is Al_3O_2, and the tetrahedral (T) site is 2[SiO_4]. Here Fe^{3+} is estimated by charge balance criteria. At low Fe^{3+}, the OH site is close to filled, but may be less than the ideal sum in Fe^{3+}-rich chloritoid, consistent with deprotonation and oxidation of Fe^{2+} to Fe^{3+} (Deer, Howie, and Zussman, 2013). While the assumption of 8 cations and 12 oxygen equivalents used here to calculate Fe^{3+} is violated at elevated Fe^{3+} (which may occupy up to 50% of R^{3+} in the L1 layers), such high Fe^{3+} chloritoid compositions are rare (Deer, Howie, and Zussman, 2013). The calculation procedure used here is expected to perform well for most chloritoid analyses. Chloritoid compositions may be plotted as either a X_{Mg} binary (with adjustable upper and lower limits) or in the Fe^{2+}-Mg-Mn ternary (Fig. 8).

3.11 Talc

The structural formula for talc ($M_3T_4O_{10}(OH)_2$) is normalized here to 11 oxygen equivalents, with K, Na, Ca, Mg, Mn, Fe^{2+}, Ni, Ti, and Al^{VI} allocated to the octahedral (M) site,

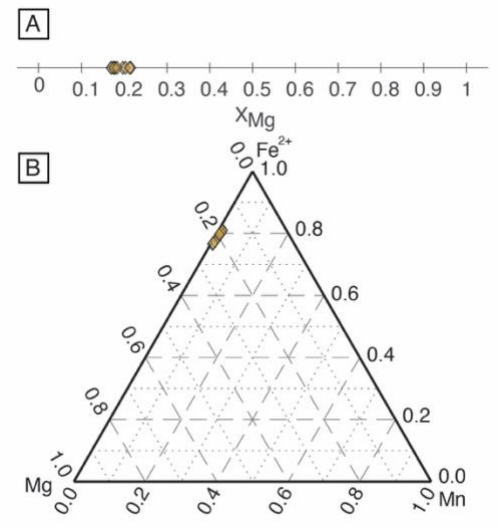

Figure 8. Binary X_{Mg} (**A**) and ternary Fe^{2+}, Mg, and Mn (**B**) compositional diagrams for chloritoid. Analytical data were collected on chloritoid inclusions in garnet cores in eclogite from As Sifah, Oman (Unpublished).

and Al^{IV} and Si on tetrahedral (T) site. Here ΣFe is assumed to be Fe^{2+}. Compositional plots are not currently offered.

3.12 Epidote group

Compositions of epidote group members are described as $A_2M_3T_3(O,OH,F)_{12}$, where K, Na, Ca, and Mg are assigned to the A site, Mn^{3+},Fe^{3+}, Cr, Ti, and Al^{IV} assigned to the octahedral M site, and Al and Si assigned to the tetrahedral T site. The most abundant epidote group minerals fall between the (clino-)zoisite ($Ca_2Al_3Si_3O_{11}O(OH)$) and epidote ($Ca_2Al_2Fe^{3+}Si_3O_{11}O(OH)$) endmembers. While the exchange vectors with peimontite ($Ca_2Al_2Mn^{3+}Si_3O_{11}O(OH)$) and tawmawite ($Ca_2Al_2CrSi_3O_{11}O(OH)$) are considered here, the substitutions of Ce, Sr, Pb, La, Y and Th on the A site are not currently implemented in MinPlot. All Fe and Mn are assumed to be trivalent. Endmembers fractions are expressed as (clino-)zoisite (X_{Czo} = (Al^{VI}-2)/(Fe^{3+} + Al^{VI} + Cr + Mn^{3+} - 2)), epidote (X_{Ep} = Fe^{3+}/(Fe^{3+} + Al^{VI} + Cr + Mn^{3+} - 2)), piemontite (X_{Pmt} = Mn^{3+}/(Fe^{3+} + Al^{VI} + Cr + Mn^{3+} - 2)), and tawmawite ($X_{Taw.}$ = Fe^{3+}/(Fe^{3+} + Al^{VI} + Cr + Mn^{3+} - 2). Epidote compositions are plotted in an Al-Fe^{3+} binary diagram, similar to plots offered for olivine (Fig. 3a) and chloritoid (Fig. 8a).

3.13 Titanite

Titanite ($CaTiSiO_5$) has three structural sites and may display significant compositional variability. The 7-fold decahedral site may incorporate K, Na, Y, and Ca, the octahedral site may incorporate Mg, Mn, Fe^{3+}, Ti, and Al^{VI}, and the tetrahedral site contains Si and Al^{IV}. Rare Earth elements, Sr, Pb, and U may also substitute into the decahedral site, as well as Zr, Nb, and Ta on the octahedral site, but are not considered here due to their relatively low abundance in most titanite. Here, all Fe is considered as Fe^{3+} and titanite are normalized to fully occupied octahedral and tetrahedral sites:

(10) $$NF^C = \frac{2}{\sum_i^Z n_{Oct}^C + \sum_i^Z n_T^C}$$

Where NF^C is the cation-based normalization factor, $\sum_i^Z n_{Oct}^C$ is the sum of Mg, Mn, Fe^{3+}, Ti, and Al^{VI}, and $\sum_i^Z n_T^C$ is the sum of Si and Al^{IV}. Fluorine and OH^- are thought to substitute for O via the exchange vector $(Al,Fe)^{3+}$ + $(OH,F)^-$ = Ti^{4+} + O^{2-} (see review in Kohn, 2017). Fluorine may be measured by directly EPMA, whereas OH is calculated as OH = (Al^{VI} + Fe^{3+}) – F. Oxygen is calculated as the sum of the cation charges minus 0.5(F + OH). Finally, the fraction of titanite is calculated as X_{Ttn} = Ti/$\sum_i^Z n_{Oct}^C$. Currently no plotting options are available for titanite.

3.14 Spinel

Spinel group minerals ($A^{2+}B_2^{3+}O_4$) are calculated here to 3 cations and 4 oxygen equivalents for Fe^{3+} estimation. Magnesium, Mn, Fe^{2+}, Zn, and Ni are assigned to the tetrahedral (A) site, whereas Fe^{3+}, Cr, Al, and Ti substitute on the octahedral (B) site. Spinel compositions are

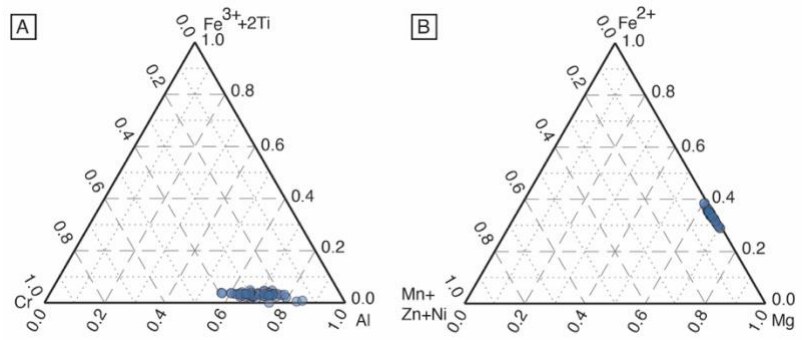

Figure 9. Ternary Fe^{3+} + 2Ti, Al, and Cr (**A**) and Fe^{2+}, Mg, and Mn + Zn + Ni (**B**) diagrams for spinel. Data are analyses of spinnel from mantle peridotite, Wadi Fins, Oman (de Obseso and Kelemen, 2020).

plotted in the Cr, Fe^{3+} + 2Ti, and Al and Fe^{2+}, Mg, and Mn + Zn + Ni ternary diagrams (Fig. 9a and b, respectively).

3.15 Sulfides

A generic procedure is available for sulfide minerals. The datafile requires the mass fractions (in wt. %) for S, Co, Cu, As, Fe, Ni, Pb, and Zn. All elements, except for S, are optional, allowing the maximum flexibility for a variety of sulfides. There are multiple options for normalization. First, the user is asked to specify if they want to normalize on a cation or anion basis. Cation normalization works well for many sulfides but should not be done for pyrrhotite ($Fe_{1-X}S$) where the cation total is not fixed. Second, As (–3 to +5) can be treated either as a cation or an anion. On the reduced end As^{1-} may substitute for S_2^{2-} anion in pyrite and other disulfides. However, at more oxidizing conditions As^{2+} and As^{3+} may substitute for divalent and trivalent cations (e.g., Deditus *et al*., 2008; Qian *et al*., 2013). Trends in Fe-As-S ternary space may be used to determine whether As should be treated as a cation or anion for a given analysis (e.g., Deditus *et al*., 2014). Currently no compositional diagrams are available for sulfide phases.

Conclusions

Electron probe microanalysis is a powerful tool for measuring raw concentrations of major and minor elements in geological materials; however, the identification of geologically important compositional trends requires formula recalculation of the raw EPMA data. MinPlot is a MATLAB®-based program, which runs on a central script that calls multiple recalculation and plotting procedures for 15 mineral groups. Due to the modular nature of MinPlot, adding additional functions for new minerals is simple, allowing the program to be easily modified and updated to include new minerals and data visualization procedures. MinPlot is also anticipated to be compatible with future releases of MATLAB®, whereas many older mineral formula recalculation programs are no longer in use because they are unsupported on modern operating systems. Finally, MinPlot provides publication ready compositional plots for most common minerals. By coding MinPlot using the MATLAB® programming language, the user is required to have a license; however, a web-based Python or R version will be released in the near future, providing increased access to MinPlot without additional cost.

Acknowledgements

MinPlot would not have been possible without a lot of help along the way. I sincerely thank Martin Yates, Heidi Höfer, Dominik Hezel, Christopher Mattinson, Mike Dorias, and Owen Neill for their guidance and training on the EPMA over the years. I would also like to thank Edward S. Grew, Horst R. Marschall, John Schumacher, Guillaume Bonnet, Guillaume Siron, and many others for their helpful and interesting discussions on mineral chemistry and mineral formula recalculation.

References

Afifi, A.M., & Essene, E. (1988). MINFILE: A microcomputer program for storage and manipulation of chemical data on minerals. *American Mineralogist*, 73, 446-448.

Bernhardt, H.J. (2010). MINCALC-V5, a non EXCEL based computer program for general electron-microprobe mineral analyses data processing. *IMA 20th General Meeting 2010, Acta Mineralogy and Petrology Abstract Series*, 6, 869.

Brandelik, A (2009). CALCMIN – an EXCELTM Visual Basic application for calculating mineral structural formulae from electron microprobe analyses. *Computers & Geosciences*, 35, 1540-1551.

De Angelis, S.M.H., & Niell, O.K. (2012). MINERAL: A program foor the propagation of analytical uncertainty through mineral formula recalculations. *Computers & Geosciences*, 48, 134-142.

Deditius, A.P., Reich, M., Kesler, S.E., Utsunomiya, S., Chryssoulis, S.L., Walshe, J., & Ewing, R.C. (2014). The coupled geochemistry of Au and As in pyrite from hydrothermal ore deposits. *Geochimica et Cosmochimica Acta*, 140, 644-670.

Deditius, A.P., Utsunomiya, S., Renock, D., Ewing, R.C., Ramana, C.V., Becker, U., & Kesler, S.E. (2008). A proposed new type of arsenian pyrite: Composition, nanostructure and geological significance. *Geochimica et Cosmochimica Acta*, 72, 2919-2933.

De Bjerg, S.C., Mogessie, A., & Bjerg, E. (1992). HYPER-FORM – A Hypercard® program for Macintosh® microcomputers to calculate mineral formulae from electron microprobe and wet chemical analysis. *Computers & Geosciences*, 30, 909-923.

De Bjerg, S.C., Mogessie, A., & Bjerg, E. (1995). PASFORM – A program for IBM® PC or PC-compatible computers to calculate mineral formulae from electron microprobe and wet-chemical analysis. *Computers & Geosciences*, 21, 1187-1190.

Deer, W.A., Howie, R.A., & Zussman, J. (2013). An introduction to the rock-forming minerals. London: The Mineralogical Society.

De Obeso, J.C., & Kelemen, P.B. (2020). Major element mobility during serpentinization, oxidation and weathering of mantle peridotite at low temperatures. *Philosophical Transactions of the Royal Society A*, 378, 20180433.

Esawi, E.K. (2004). AMPH-CLASS: An Excel spreadsheet for the classification and nomenclature of amphiboles based on the 1997 recommendations of the International Mineralogical Association. *Computers and Geosciences*, 30, 753-760.

Forshaw, J.B., & Pattison, D.R.M. (2021). Ferrous/ferric (Fe2+/Fe3+) partitioning among silicates in metapelites. Contributions to Mineralogy and Petrology, 176, 1-26.

Grew, E.S., Locock, A.J., Mills, S.J., Galuskina, I.O., Galuskin, E.V., & Hålenius, U. (2013). Nomenclature of the garnet supergroup. *American Mineralogist*, 98, 785-811.

Hawthorne, F.C., Oberti, R., Harlow, G.E., Maresch, W.V., Martin, R.F., Schumacher, J.C., & Welch, M.D. (2012). Nomenclature of the amphibole supergroup. *American Mineralogist*, 97, 2031-2048.

Hawthorne, F.C., Ungaretti, L., Oberti, R., Caucia, F., & Callegari, A. (1993). The crystal chemistry of staurolite. I. Crystal structure and site populations. The Canadian Mineralogist, 31, 551-582.

Holdaway, M.J., Mukhopadhyay, B., Dyar, M.D., Dutrow, B.L., Rumble, D., & Grambling, J.A. (1991). A new perspective on staurolite crystals chemistry: Use of stoichiometric and chemical end-members for a mole fraction model. *American Mineralogist*, 76, 1910-1991.

Knowles, C.R. (1987). A BASIC program to recast garnet end-members. *Computers & Geosciences*, 13, 655-659.

Kohn, M.J. (2017). Titanite petrochronology. *Reviews in Mineralogy and Geochemistry*, 83, 419-441.

Leake, B.E., Woolley, A.R., Arps, C.E.S., Birch, W.D., Gilbert, M.C., Grice, J.D., Hawthorne, F.C., Kato, A., Kish, H.J., Krivovichev, V.G., Linthout, K., Laird, J., Mandarino, J.A., Maresch, W.V., Nickel, E.H., Rock, N.M.S., Schumacher, J.C., Smith, D.C., Stephenson, N.C.N., Ungaretti, L., Whittaker, E.J.W., & Youzhi, G. (1997). Nomenclature of amphiboles: Report of the subcommittee on amphiboles of the International Mineralogical Association, Commission on New Minerals and Mineral Names. *The Canadian Mineralogist*, 35, 219-246.

Li, X., Zhang, C., Behrens, H., & Holtz, F. (2020). Calculating biotite formula from electron microprobe analysis data using a machine learning method based on principal components regression. Lithos, 356-357: 105371.

Le Pioufle, A., & Canil, D. (2012). Iron in monticellite as an oxygen barometer for kimberlite magmas. *Contributions to Mineralogy and Petrology*, 163, 1033-1046.

Locock, A.J. (2008). An Excel spreadsheet to recase analyses of garnet into end-member components, and a synopsis of the crystal chemistry of natural silicate garnets. *Computers & Geosciences*, 62, 1-14.

Lockock, A.J. (2014). An Excel spreadsheet to classify chemical analyses of amphibole following the IMA 2012 recommendations. *Computers & Geosciences*, 62, 1-14.

Masci, L., Dubacq, B., Verlaguet, A., Chopin, C., de Andrade, V., & Herviou, C. (2019). A XANES and EPMA study of Fe^{3+} in chlorite: Importance of oxychlorite and implications for cation site distribution and thermobarometry. *American Mineralogist*, 104, 403-417.

Meija, J., Coplen, T.B., Berglund, M., Brand, W.A., De Bièvre, P., Gröning, M., Holden, N.E., Irrgeher, J., Loss, R.D., Walczyk, T., & Prohaska, T. (2016). Atomic weights of the elements 2013 (IUPAC Technical Report). *Pure and Applied Chemistry*, 88, 265-291.

Mogessie, A, Tessadri, R., & Veltman, C.B. (1990). EMP-AMPH – a Hypercard program to determine the name of an amphibole from electron microprobe analysis according to the International Mineralogical Association scheme. *Computers and Geosciences*, 16, 309-330.

Mogessie, A. (2001). AMPH-IMA97: a Hypercard program to determine the name of an amphibole from electron microprobe and wet chemical analyses. *Computers and Geosciences*, 27, 1171-1180.

Morimoto, N., Fabries, J., Fergusson, A.K., Ginzburg, I.V., Ross, M., Seifert, F.A., Zussman, J., Aoki, K., & Gottardi, G. (1989). Nomenclature of pyroxenes. *Mineralogical Journal*, 14, 198-221.

Oberti, R., Ungretti, L., Cannnillo, E., & Hawthorne, F.C. (1992). The behaviour of Ti in amphiboles. I. Four- and six-coordinate Ti in richterite. *European Journal of Mineralogy*, 4, 425-439.

Piccardo, G.B., & Guarnieri, L. (2011). Gabbro-norite cumulates from strongly depleted MORB melts in the Alpine-Apennine ophiolites. *Lithos*, 124, 200-214.

Qian, G., Brugger, J., Testemale, D., Skinner, W., & Pring, A. (2013). Formation of As(II)-pyrite during experimental replacement of magnetite under hydrothermal conditions. *Geochimica et Cosmochimica Acta*, 100, 1-10.

Rao, D.R., & Rao, T.V.S. (1996). AMPH: A program for calculating formulae for assigning names to the amphibole group of minerals. *Computers & Geosciences*, 22, 931-933.

Richard, L.R., & Clarke, D.B. (1990). AMPHIOBOL: A program for calculating structural formulae and for classifying and plotting chemical analyses of amphiboles. *American Mineralogist*, 75, 421-423.

Rock, N.M.S., & Carroll, G.W. (1990). MINTAB: A general-purpose mineral recalculation and tabulation program for Macintosh. *American Mineralogist*, 75, 424-430.

Rock, N.M.S. (1987). A FORTRAN program for tabulating and naming amphibole analyses according to the International Mineralogical Association scheme. *Mineralogy and Petrology*, 37, 79-88.

Rock, N.M.S., & Leake, R.E. (1984). The International Mineralogical Association amphibole nomenclature scheme: Computerization and its consequences. *Mineralogical Magazine*, 48, 211-227.

Schumacher, J.C. (1991). Empirical ferric iron corrections: Necessity, assumptions, and effects on selected geothermobarometers. *Mineralogical Magazine*, 55, 3-18.

Spear, F.S., & Kimball, K.L. (1984). RECAMP – A FORTRAN IV program for estimating Fe3+ contents in amphiboles. *Computers in Geology*, 10, 317-325.

Spreitzer, S.K., Walters, J.B., Cruz-Uribe, A.M., Williams, M.L., Yates, M.G., Jercinovic, M.J., Grew, E.S., & Carson, C.J. (2021). Monazite petrochronologgy of polymetamorphic granulite-facies rocks of the Larsemann Hills, Prydz Bay, East Antarctica. *Journal of Metamorphic Geology*, 39, 1205-1228.

Sturm, R. (2002). PX-NOM – An interactive spreadsheet program for the computation of pyroxene analyses derived from the electron microprobe. *Computers & Geosciences*, 28, 473-483.

Tiepolo, M., Zanetti, A., & Oberti, R. (1999). Detection, crystal-chemical mechanisms and petrological implications of $^{[6]}Ti^{4+}$ partitioning in pargasite and kaersutite. *European Journal of Mineralogy*, 11, 345-354.

Tindle, A.G., & Webb, P.C. (1994). Probe-AMPH – A spreadsheet program to classify microprobe-derived amphibole analyses. *Computers & Geosciences*, 20, 1201-1228.

Xu, J., Zhang, G.B., Marschall, H.R., Walters, J.B., Liu, S.Q., Lü, Z., Zhang, L.F., Hu, H., & Li, N. (2022). Boron isotopes of white mica and tourmaline in an ultra-high pressure metapelite from the western Tianshan, China: Dehydration and metasomatism during exhumation of subducted ocean-floor sediments. *Contributions to Mineralogy and Petrology*, 177 (46), 1-16.

Yavuz, F (2003a). Evaluating micas in petrologic and metallogenic aspect: I – definitions and structure of the computer program MICA^{+}. *Computers & Geosciences*, 29, 1203-1213.

Yavuz, F (2003b). Evaluating micas in petrologic and metallogenic aspect: II – applications using the computer program MICA^{+}. *Computers & Geosciences*, 29, 1215-1228.

Yavuz, F (2007). WinAmphcal: A windows program for the IMA-04 amphibole classification. *Geochemistry, Geophysics, Geosystems*, 8, Q01004.

Yavuz, F (2013). WinPyrox: A Windows program for pyroxene calculation classification and thermobarometry. *American Mineralogist*, 98, 1338-1359.

Yavuz, F., Kumral, M., Karakaya, N., Karakaya, M.C., & Yildirim, D.K. (2015). A windows program for chlorite calculation and classification. *Computers & Geosciences*, 81, 101-113.

Yavuz, F., & Yildirim, D.K. (2020). WinGrt, a Windows program for garnet supergroup minerals. *Journal of Geosciences*, 65, 71-95.

Walters, J.B., Cruz-Uribe, A.M., & Marschall, H.R. (2019). Isotopic compositions of sulfides in exhumed high-pressure terranes: Implications for sulfur cycling in subduction zones. *Geochemistry, Geophysics, Geosystems*, 20, 2019GC008374.

Walters, J.B., Cruz-Uribe, A.M., Marschall, H.R., & Boucher, B. (2021). The role of sulfides in the chalcophile and siderophile element budget of the subducted oceanic crust. *Geochimica et Cosmochimica Acta*, 304, 191-215.

Walters, J.B., Cruz-Uribe, A.M., Song, W.J., Gerbi, C., & Biela, K. (2022). Strengths and limitations of in situ U-Pb titanite petrochronology in polymetamorphic rocks: An example from western Maine, USA. *Journal of Metamorphic Geology*, 40, 1043-1066.

Walters, J.B., & Kohn, M.J. (2017). Protracted thrusting followed by late rapid cooling of the Greater Himalayan Sequence, Annapurna Himalaya, Central Nepal: Insights from titanite petrochronology. *Journal of Metamorphic Geology*, 35, 897-917.